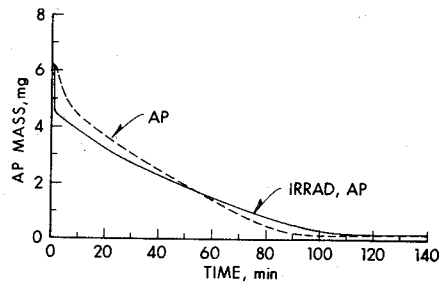

Fig. 1 Isothermal heating curve of irradiated and unirradiated AP at 576K.

when comparing the irradiated AP to the unirradiated sample. All kinetic runs were made in a flowing argon atmosphere.

Results

Figure 1 compares individual kinetic runs of the irradiated and unirradiated AP. The nearly vertical portion at the beginning of each run is the weight loss from the low-temperature decomposition. One can see in Fig 1 that the initial weight loss is more rapid for the irradiated AP and that the fraction of AP decomposing via the low-temperature path is slightly greater for the irradiated AP. Such observations are in accord with previous results.[7,8] The remaining portion of each kinetic run corresponds to the vaporization of AP which continues until all the AP is consumed. To see the effect of neutron radiation on the vaporization of AP, the weight loss corresponding to the vaporization of AP was converted to fraction reacted α and the fraction reacted vs time fit to several equations representing solid-state decomposition kinetics.[16] In accord with Jacobs and Russell-Jones,[15] the following equation was found to best represent the fraction reacted vs time

$$1-(1-\alpha)^{1/2}=kt$$

The rate coefficient k was calculated by a linear least-squares fit of $f(\alpha)$ vs t. Table 1 summarizes the rate coefficients computed in this fashion for all the kinetic runs we performed. Clearly the rate of vaporization of the irradiated AP is the same as the rate of vaporization of the unirradiated sample.

Conclusion

The vaporization rate of AP is unaffected by a neutron fluence of 4×10^{14} neutrons/cm^2, although the low-temperature decomposition is altered by the same fluence. One would expect the neutrons to primarily affect condensed phase reactions. The literature indicates that the rate of vaporization is the only condensed phase reaction deemed important in the AP combustion. Therefore one would expect a neutron fluence of 4×10^{14} neutrons/cm^2 to have no effect on the combustion rate of AP or the combustion rate of composite propellant made from irradiated AP.

References

[1] Freeman, E.S., Anderson, D.A., and Campisi, J.J., "The Effects of X-Ray and Gamma-Ray Irradiation of the Thermal Decomposition of Ammonium Perchlorate in the Solid State," *Journal of Physical Chemistry*, Vol. 64, No. 11, Nov. 1960, pp. 1727-1732.

[2] Herley, P.J. and Levy, P.W., "Thermal Decomposition of Irradiated Orthohombic Ammonium Perchlorate," *Nature*, Vol. 211, Sept. 1966, pp. 1287-1288.

[3] Herley, P.J. and Levy, P.W., "Effects of X-Ray and γ-Ray Radiation on the Thermal Decomposition of Solid Orthorhombic Ammonium Perchlorate. I. Experimental Results," *Journal of Chemical Physics*, Vol. 49, No. 4, Aug. 1968, pp. 1493-1500.

[4] Herley, P.J. and Levy, P.W., "Effects of X-Ray and γ-Ray Radiation on the Thermal Decomposition of Solid Orthorhombic Ammonium Perchlorate. II. Kinetics and Discussion," *Journal of Chemical Physics*, Vol. 49, No. 4, Aug. 1968, pp. 1500-1509.

[5] Folger, S. and Lawson, D., "γ-Irradiation Effects on the Thermal Stability and Decomposition of Ammonium Perchlorate," *Journal of Physical Chemistry*, Vol. 74, No. 7, April 1970, pp. 1637-1639.

[6] Levy, P.W. and Herley, P.J., "Effect of Radiation on the Thermal Decomposition Induction Period in Ammonium Perchlorate and Other Pseudostable Materials," *Journal of Physical Chemistry*, Vol. 75, No. 2, Jan. 1971. pp. 191-201.

[7] Herley, P.J., Wang, C.S., Varsi, G., and Levy, P.W., "Effect of Fast Neutron, Gamma-Ray, and Combined Radiations on the Thermal Decomposition of Ammonium Perchlorate Single Crystals," *Journal of Chemical Physics*, Vol. 60, No. 6, March 1974, pp. 2430-2439.

[8] Ward, J.R., Rocchio, J.J., and Decker, L.J., "Effect of Neutron Irradiation on Military-Grade Ammonium Perchlorate," BRL Memorandum Rept. 2448, March 1975, U.S. Army Ballistic Research Labs., Aberdeen Proving Ground, Md.

[9] Caveny, L.H. and Pittman, C.U., "Contribution of Solid-Phase Heat Release to AP Composite-Propellant Burning Rate," *AIAA Journal*, Vol. 6, No. 8, Aug. 1968, pp. 1461-1467.

[10] Schmidt, W.G., "The Effect of Solid Phase Reactions on the Ballistic Properties of Propellants," NASA CR-111940, Sept. 1970.

[11] Kiselev, A.N., Plyusnim, V.I., Boldyrev, A.V., Deribas, A.A., and Boldyrev, V.V., "Effect of Preliminary Treatment of Ammonium Perchlorate by a Shock Wave on its Rate of Thermal Decomposition and Burning of Mixtures on its Base," *Combustion, Explosions and Shock Waves*, Vol. 8, No. 4, Oct. 1972, pp. 595-597.

[12] Northan, G.B. Pellet, G.L., and Cofer, W.R., "Effects of Low-Temperature Ammonium Perchlorate Decomposition on the B Ballistic Properties of a CTPB Propellant," *AIAA Journal*, Vol. 10, No. 8, Aug. 1972, pp. 1068-1072.

[13] Boggs, T.L., Zurn, D.E., and Cordes, H.F., "The Combustion of Ammonium Perchlorate and Various Inorganic Additives," AIAA Paper 75-233, Jan. 1975.

[14] Guirao, G. and Williams, F.A., "Models for the Sublimation of Ammonium Perchlorate," AIAA Paper 69-22, April 1969.

[15] Jacobs, P.W.M., and Russell-Jones, A., "Sublimation of Ammonium Perchlorate," *Journal of Physical Chemistry*, Vol. 72 No. 1, Jan. 1968, pp. 202-207.

[16] Hancock, J.D. and Sharp, J.H., "Method of Comparing Solid-State Kinetic Data and Its Application to the Decomposition of Kaolinite, Brucite, and $BaCO_3$," *Journal of the American Ceramic Society*, Vol. 55, No. 2, Feb. 1972, pp. 74-77.

Dynamic Response of Laminated Composite Plates under Initial Stress

C. T. Sun*
Iowa State University, Ames, Iowa
and
J. M. Whitney†
Wright-Patterson Air Force Base, Ohio

Introduction

IT is a well known fact that an initial stress will modify the mechanical properties of a medium. As an example, a homogeneous and isotropic medium in the unstressed state may become nonhomogeneous and anisotropic under initial stress. In general, a tensile initial stress will stiffen the rigidity of the medium, while a compressive initial stress will

Received May 19, 1975; revision received September 22, 1975. This work was supported by the Engineering Research Institute, Iowa State University. The authors wish to thank W. L. Whitford of the Aeronautical Systems Division, Wright-Patterson Air Force Base for assistance in the numerical computations.

Index categories: Structural Composite Materials; Structural Dynamic Analysis.

*Associate Professor, Department of Engineering Science and Mechanics and Engineering Research Institute.

†Materials Engineer, Air Force Materials Laboratory. Associate Fellow AIAA.

Table 1 Dynamic load factors, $\theta = 45°$

$\bar{N}_0$	w			$\psi_{x,x}$			$\psi_{y,x}$		
	Case 1	Case 2	Case 3	Case 1	Case 2	Case 3	Case 1	Case 2	Case 3
0	2.00	1.75	1.90	1.97	1.70	1.88	1.54	1.11	1.31
0.01	1.88	1.48	1.75	1.82	1.30	1.50	1.39	1.08	1.22
0.02	1.46	1.26	1.30	1.46	1.10	1.26	1.19	1.01	1.08
0.03	1.16	1.07	1.11	1.15	1.06	1.07	1.07	1.00	1.04

Table 2 Dynamic load factors, $\theta = 90°$

$\bar{N}_0$	w			$\psi_{x,x}$		
	Case 1	Case 2	Case 3	Case 1	Case 2	Case 3
0	1.99	1.70	1.87	1.92	1.65	1.80
0.01	2.37	1.85	2.19	2.12	1.77	1.95
0.02	2.72	2.14	2.52	2.24	1.85	2.01
0.03	2.93	2.44	2.70	2.30	1.94	2.10

reduce its rigidity. When the compressive initial stress reaches a critical value, the rigidity of the medium becomes very small, and instability will occur.

The stability problems of plates and shells under compressive initial stress have been investigated by many distinguished researchers. The objective of this Note is to investigate the effects of initial tensile stress on the dynamic response of an infinitely long, simply supported composite plate under cylindrical bending. The investigation is carried out by using a method previously developed by the authors[1] to analyze composite plates under time-dependent dynamic pressure. This method was first established by Mindlin and Goodman[2] and was extended by Yu[3] to the investigation of sandwich plates.

Governing Equations

Consider a laminated plate of thickness h with the origin of Cartesian coordinate system located within the central plane $(x-y)$ with the z-axis being normal to this plane. For cylindrical bending in the x-direction, the laminated plate theory used in Ref. 1 is based on the assumed displacement field

$$u = u^0(x,t) + z\psi_x(x,t)$$
$$v = v^0(x,t) + z\psi_y(x,t) \qquad (1)$$
$$w = w(x,t)$$

where u^0 and v^0 are the displacement components of the middle surface $(z=0)$ in x, y directions, respectively, w is the transverse displacement, and ψ_x and ψ_y represent the rotations of a normal to the middle surface about the y and x axes, respectively. For the case of an initial stress resultant $N_x = N_0 = \text{constant}$, Eq. (3) of Ref. 1 becomes, with partial differentiation denoted by a comma

$$k[A_{55}\psi_{x,x} + A_{45}\psi_{y,x} + (A_{55} + N_0)w_{,xx}]$$
$$+ p = Pw_{,tt} \qquad (2)$$

where A_{ij}, k, p, and P denote plate stiffnesses, shear correction factor, surface pressure, and integral of the density through the plate thickness, respectively. The remaining equations of motion are unchanged by the introduction of N_0. Since the only effect of the initial tensile stress resultant is an increase in the stiffness coefficient of $w_{,xx}$, the solution to the governing equations in terms of separation of variables and the Mindlin-Goodman procedure[2] as presented in Ref. 1 is applicable to the present problem. The details of this solution method are not repeated here.

Three cases of time-dependent dynamic loading are considered for an infinitely long plate simply supported at the ends $x=0, L$, under a concentrated load $P(x,t) = P_0F(t)$ at the center $X = L/2$.

Case 1

$$F(t) = H(t - t_1) \qquad (3)$$

Case 2

$$F(t) = t/t_1 \qquad 0 \le t \le t_1$$
$$= 2 - t/t_1 \qquad t_1 \le t \le 2t_1 \qquad (4)$$
$$= 0 \qquad t \ge 2t_1$$

Case 3

$$F(t) = \sin \pi t/t_1 \qquad 0 \le t \le t_1$$
$$= 0 \qquad t \ge t_1 \qquad (5)$$

Loading Case 1 represents a rectangular pulse between $t=0$ and $t=t_1$, Case 2 a triangular pulse, and Case 3 a sine pulse.

Numerical Results

Numerical results for the displacement variables are obtained for eight-layer $0/0/\theta/-\theta/-\theta/\theta/0/0$ graphite/epoxy laminates having the same unidirectional properties as in Ref. 1. The maximum deflection and inplane stresses occur at $x = L/2$ and $t = T_1$. The maximum value of the interlaminar shear, τ_{xz}, occurs at $x = 0, L$ and $t = T_2$. The evaluation of T_1 and T_2 for each case is obtained by plotting the appropriate

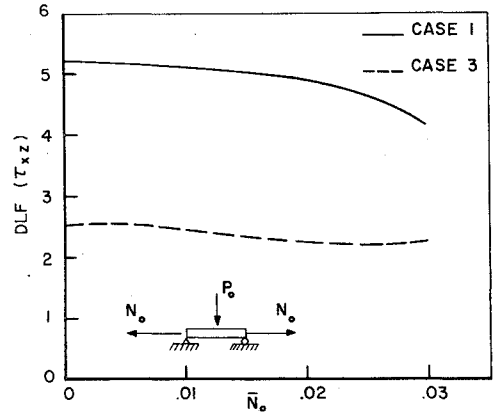

Fig. 1 Dynamic load factor for interlaminar shear stress τ_{xz} as a function of $\bar{N}_0$ for the case $\theta = 45°$.

variable as a function of t. The angle θ in each ply is the angle between the fiber direction and x-axis of the plate. It is also assumed that $L/h=20$ and the dwell time $\bar{T}_1=100$ where $\bar{T}_1=(E_T/\rho h^2)t_1$ with E_T denoting the modulus of a unidirectional layer transverse to the fiber direction and ρ denoting laminate density. Dynamic load factors (ratio of dynamic solution to static solution) are presented in Tables 1 and 2 for increasing values of N_0 (shown in the non-dimensional form $\bar{N}_0=N_0/E_T h$). These results correspond to $\theta=45°$ and 90° respectively. Maximum in-plane stresses for the ith layer of the laminate can be calculated from the relations‡

$$\sigma_x^i=Q_{11}^i u_x^0+z(Q_{11}^i\psi_{xx}+Q_{16}^i\psi_{y,x})$$

$$\sigma_y^i=Q_{12}^i u^0{}_{,x}+z(Q^i{}_{12}\psi_{x,x}+Q^i{}_{26}\psi_{y,x})$$

$$\tau_{xy}^i=Q_{16}^i u^0{}_{,x}+z(Q^i{}_{16}\psi_{x,x}+Q^i{}_{66}\psi_{y,x}) \qquad (6)$$

where Q_{ij} are the anisotropic reduced stiffnesses for plane stress. For the present plate theory in which the effects of transverse shear deformation are included the inplane stresses are not a function of w explicitly. It should not noted, however, that through the coupling of w, ψ_x, and ψ_y in the governing equations the inplane stresses are indirectly related to w. For the symmetric laminates discussed in the present work, $u_{,x}{}^0$ is a constant proportional to N_0. Thus, w, ψ_x, and ψ_y are the only time dependent variables. It should be noted that the laminates under discussion display orthotropic in-plane properties *(i.e.,* $A_{16}=A_{26}=0$) resulting in the vanishing of v^0. The interlaminar shear stress τ_{xz} can be determined by using Eqs. (6) in conjunction with the dynamic theory of elasticity in the following manner

$$\tau_{xz}^i=-\int_{-h/2}^{z}(\sigma^i{}_{x,x}-\rho z\psi_{x,tt})\,dz \qquad (7)$$

The dynamic load factor for the maximum value of τ_{xz} is shown in Fig. 1 for $\theta=45°$ and $z=0$. It should be noted that, depending on layer properties, the maximum value of τ_{xz} does not always occur at the laminate mid-plane. Similarly, the maximum value of the in-plane stresses does not always occur at the outer surface of the plate. It should also be noted that for $\theta=90°$, ψ_y vanishes.

A cursory examination of the numerical results reveals that an initial in-plane tensile stress resultant has considerable influence on the dynamic load factor. The exact character of the change, i.e., increase or decrease, depends on the orientation in the laminate.

References

[1] Sun, C. T. and Whitney, J. M., "Forced Vibrations of Laminated Composite Plates in Cylindrical Bending," *The Journal of the Acoustical Society of America*, Vol. 55, May 1974, pp. 1003-1008.

[2] Mindlin, R. D. and Goodman, L. G., "Beam Vibrations with Time-Dependent Boundary Conditions," *Journal of Applied Mechanics*, Vol. 17, 1950, pp. 377-380.

[3] Yu, Y. Y., "Forced Flexural Vibrations of Sandwich Plates in Plane Strain," *Journal of Applied Mechanics*, Vol. 27, 1960, pp. 535-540.

‡In general the peak values for $\psi_{x,x}$ and $\psi_{y,x}$ do not occur at the same instant. Since the numerical values for $\psi_{x,x}$ are at least ten times greater than $\psi_{y,x}$ and $Q^i{}_{11}$ and $Q^i{}_{16}$ are in the same order of magnitude, it follows that for practical applications the dynamic load factors for the inplane stresses are very close to the dynamic load factor for $\psi_{x,x}$.

Near-Field Studies of a Choked Jet Seeded with Upstream Sound

B.H.K. Lee*
National Research Council, Ottawa, Ontario, Canada

Introduction

A NUMBER of studies[1-4] on core engine noise have been published in recent years. There is substantial evidence[1,2] that the noise from low-velocity jets cannot be accounted for by Lighthill's theory alone. Internally generated noise upstream of the nozzle contributes significantly to the overall noise radiated by the jet. As early as 1953, Mawardi and Dyer[5] reported measurements on turbojet engine noise and found the velocity index to vary from 4 to 8 as the thrust was increased. The importance of internal noise has been overlooked for many years, and, in testings of jet engines, the deviation from the U^8 law was regarded as an imperfection of the engine rather than a fundamental effect.

In spite of some recent investigations by engine manufacturers and independent researchers, the subject of internal noise is still poorly understood. This is because of the complexity of the problem, and more fundamental studies are required to identify the internal noise sources, the coupling between them, and the transmission characteristics as a function of the jet flow.

To study the transmission of core noise, it is desirable to introduce sound of controllable amplitude and frequency upstream of the nozzle and to follow the development of the radiated waves and the modification by the jet flow in the near field. This paper presents some preliminary observations in the near field of a 2¼-in. cold choked jet seeded with high-intensity sound waves of discrete frequencies generated by an annular cavity cut into the inside surface of a nozzle. Microphone traverses at a frequency of 12.5 kHz have been carried out. This frequency corresponds to the fundamental of the internally generated waves, with the cavity width set at ½ in. The results for other cavity widths exhibit behavior similar to that reported herein, and detailed measurements at other frequencies are reported in Ref. 6.

Experiments

The experimental facility used in the present experiments has been described by Westley and Woolley.[7] The nozzle used in the experiments has an inside diameter D of 2.25 in. and a parallel length of 4.2 in. It was connected to a 6-in-diam air supply pipe by a converging section. Figure 1 shows a cross section of the nozzle. An annular cavity was cut on the inside surface of the nozzle at a distance $d=½$ in. from the exit. The cavity depth h was kept constant at ¼ in., and the width b could be varied from ⅛ to ½ in. The dimension for the nozzle wall thickness t was ⅜ in.

A ¼-in.-diam condenser microphone (B&K 4135) was mounted on a lathe bed drive and could be motor-driven at a speed of approximately 1 ips, for a distance up to 30 in. The near-field traverses of the sound pressure level at frequencies corresponding to those generated by the cavity were obtained by feeding the microphone signals through a B&K ⅓-octave frequency analyzer.

Optical studies of the jet flow and the sound field were obtained by a single-pass schlieren system with a nanolite source (model K30) and two spherical mirrors of 3-ft diam and 24-ft focal length. A microphone was used to trigger the light

Received May 22, 1975; revision received Oct. 9, 1975.
Index categories: Jets, Wakes, and Viscid-Inviscid Flow Interactions; Aircraft Noise, Aerodynamics (Including Sonic Boom).

*Associate Research Officer, National Aeronautical Establishment.